PCCP

Physical Chemistry Chemical Physics

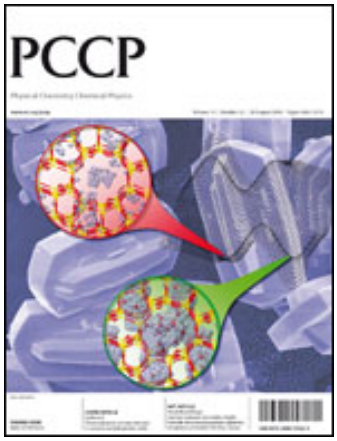

This paper is published as part of a PCCP Themed Issue on:

Water at interfaces

Guest Editor: Martin McCoustra

Editorial

Communications

Papers

Raman spectra of complexes of HNO_3 and NO_3^- with NO_2 at surfaces and with N_2O_4 in solution
Michael A. Kamboures, Wytze van der Veer, R. Benny Gerber and Leon F. Phillips, *Phys. Chem. Chem. Phys.*, 2008, **10**, 4748
DOI: 10.1039/b810081k

Molecular level structure of the liquid/liquid interface. Molecular dynamics simulation and ITIM analysis of the water-CCl_4 system
Lívia B. Pártay, George Horvai and Pál Jedlovszky, *Phys. Chem. Chem. Phys.*, 2008, **10**, 4754
DOI: 10.1039/b807299j

Solvent structures of mixed water/acetonitrile mixtures at chromatographic interfaces from computer simulations
Jörg Braun, Antony Fouqueau, Raymond J. Bemish and Markus Meuwly, *Phys. Chem. Chem. Phys.*, 2008, **10**, 4765
DOI: 10.1039/b807492e

Ion spatial distributions at the liquid–vapor interface of aqueous potassium fluoride solutions
Matthew A. Brown, Raffaella D'Auria, I.-F. William Kuo, Maria J. Krisch, David E. Starr, Hendrik Bluhm, Douglas J. Tobias and John C. Hemminger, *Phys. Chem. Chem. Phys.*, 2008, **10**, 4778
DOI: 10.1039/b807041e

Trapping proton transfer intermediates in the disordered hydrogen-bonded network of cryogenic hydrofluoric acid solutions
Patrick Ayotte, Sylvain Plessis and Patrick Marchand, *Phys. Chem. Chem. Phys.*, 2008, **10**, 4785
DOI: 10.1039/b806654j

Aqueous divalent metal–nitrate interactions: hydration *versus* ion pairing
Man Xu, James P. Larentzos, Mazen Roshdy, Louise J. Criscenti and Heather C. Allen, *Phys. Chem. Chem. Phys.*, 2008, **10**, 4793
DOI: 10.1039/b807090n

Structure and dynamics of water at a clay surface from molecular dynamics simulation
Virginie Marry, Benjamin Rotenberg and Pierre Turq, *Phys. Chem. Chem. Phys.*, 2008, **10**, 4802
DOI: 10.1039/b807288d

Proton mobility in thin ice films: a revisit
Eui-Seong Moon, Chang-Woo Lee and Heon Kang, *Phys. Chem. Chem. Phys.*, 2008, **10**, 4814
DOI: 10.1039/b807730b

Thermodynamics of water intrusion in nanoporous hydrophobic solids
Fabien Cailliez, Mickael Trzpit, Michel Soulard, Isabelle Demachy, Anne Boutin, Joël Patarin and Alain H. Fuchs, *Phys. Chem. Chem. Phys.*, 2008, **10**, 4817
DOI: 10.1039/b807471b

Gas phase hydration of organic ions
Paul O. Momoh and M. Samy El-Shall, *Phys. Chem. Chem. Phys.*, 2008, **10**, 4827
DOI: 10.1039/b809440n

Water photodissociation in free ice nanoparticles at 243 nm and 193 nm
Viktoriya Poterya, Michal Fárník, Milan Ončák and Petr Slavíček, *Phys. Chem. Chem. Phys.*, 2008, **10**, 4835
DOI: 10.1039/b806865h

Electroacoustic and ultrasonic attenuation measurements of droplet size and ζ-potential of alkane-in-water emulsions: effects of oil solubility and composition
Alex M. Djerdjev and James K. Beattie, *Phys. Chem. Chem. Phys.*, 2008, **10**, 4843
DOI: 10.1039/b807623e

Gas hydrate nucleation and cage formation at a water/methane interface
Robert W. Hawtin, David Quigley and P. Mark Rodger, *Phys. Chem. Chem. Phys.*, 2008, **10**, 4853
DOI: 10.1039/b807455k

Hydration water rotational motion as a source of configurational entropy driving protein dynamics. Crossovers at 150 and 220 K
J.-M. Zanotti, G. Gibrat and M.-C. Bellissent-Funel, *Phys. Chem. Chem. Phys.*, 2008, **10**, 4865
DOI: 10.1039/b808217k

Influence of wettability and surface charge on the interaction between an aqueous electrolyte solution and a solid surface
Svetlana Guriyanova and Elmar Bonaccurso, *Phys. Chem. Chem. Phys.*, 2008, **10**, 4871
DOI: 10.1039/b806236f

Molecular dynamics study of hydrated imogolite 2. Structure and dynamics of confined water
Benoît Creton, Daniel Bougeard, Konstantin S. Smirnov, Jean Guilment and Olivier Poncelet, *Phys. Chem. Chem. Phys.*, 2008, **10**, 4879
DOI: 10.1039/b803479f

Assessing the performance of implicit solvation models at a nucleic acid surface
Feng Dong, Jason A. Wagoner and Nathan A. Baker, *Phys. Chem. Chem. Phys.*, 2008, **10**, 4889
DOI: 10.1039/b807384h

Aqueous peptides as experimental models for hydration water dynamics near protein surfaces
Cecile Malardier-Jugroot, Margaret E. Johnson, Rajesh K. Murarka and Teresa Head-Gordon, *Phys. Chem. Chem. Phys.*, 2008, **10**, 4903
DOI: 10.1039/b806995f

Melting behavior of water in cylindrical pores: carbon nanotubes and silica glasses
M. Sliwinska-Bartkowiak, M. Jazdzewska, L. L. Huang and K. E. Gubbins, *Phys. Chem. Chem. Phys.*, 2008, **10**, 4909
DOI: 10.1039/b808246d

Increased interfacial thickness of the NaF, NaCl and NaBr salt aqueous solutions probed with non-resonant surface second harmonic generation (SHG)
Hong-tao Bian, Ran-ran Feng, Yan-yan Xu, Yuan Guo and Hong-fei Wang, *Phys. Chem. Chem. Phys.*, 2008, **10**, 4920
DOI: 10.1039/b806362a

Determination of the electron's solvation site on D_2O/Cu(111) using Xe overlayers and femtosecond photoelectron spectroscopy
Michael Meyer, Julia Stähler, Daniela O. Kusmierek, Martin Wolf and Uwe Bovensiepen, *Phys. Chem. Chem. Phys.*, 2008, **10**, 4932
DOI: 10.1039/b807314g

Breakdown of hydration repulsion between charged surfaces in aqueous Cs^+ solutions
Ronit Goldberg, Liraz Chai, Susan Perkin, Nir Kampf and Jacob Klein, *Phys. Chem. Chem. Phys.*, 2008, **10**, 4939
DOI: 10.1039/b807459n

A macroscopic water structure based model for describing charging phenomena at inert hydrophobic surfaces in aqueous electrolyte solutions
Johannes Lützenkirchen, Tajana Preočanin and Nikola Kallay, *Phys. Chem. Chem. Phys.*, 2008, **10**, 4946
DOI: 10.1039/b807395c

Thermally induced mixing of water dominated interstellar ices
Daren J. Burke, Angela J. Wolff, John L. Edridge and Wendy A. Brown, *Phys. Chem. Chem. Phys.*, 2008, **10**, 4956
DOI: 10.1039/b807220e

Water hydrogen bond analysis on hydrophilic and hydrophobic biomolecule sites
Daniela Russo, Jacques Ollivier and José Teixeira, *Phys. Chem. Chem. Phys.*, 2008, **10**, 4968
DOI: 10.1039/b807551b

Hydronium and hydroxide at the interface between water and hydrophobic media
Robert Vácha, Dominik Horinek, Max L. Berkowitz and Pavel Jungwirth, *Phys. Chem. Chem. Phys.*, 2008, **10**, 4975
DOI: 10.1039/b806432f

Average molecular orientations in the adsorbed water layers on silicon oxide in ambient conditions
Anna L. Barnette, David B. Asay and Seong H. Kim, *Phys. Chem. Chem. Phys.*, 2008, **10**, 4981
DOI: 10.1039/b810309g

Interfacial water structure at polymer gel/quartz interfaces investigated by sum frequency generation spectroscopy
Hidenori Noguchi, Minowa Hiroshi, Taiki Tominaga, Jian Ping Gong, Yoshihito Osada and Kohei Uosaki, *Phys. Chem. Chem. Phys.*, 2008, **10**, 4987
DOI: 10.1039/b807297n

Co-adsorption of water and hydrogen on Ni(111)
Junjun Shan, Jacques F. M. Aarts, Aart W. Kleyn and Ludo B. F. Juurlink, *Phys. Chem. Chem. Phys.*, 2008, **10**, 4994
DOI: 10.1039/b808219g

Water–methanol mixtures: topology of hydrogen bonded network
Imre Bakó, Tünde Megyes, Szabolcs Bálint, Tamás Grósz and Viorel Chihaia, *Phys. Chem. Chem. Phys.*, 2008, **10**, 5004
DOI: 10.1039/b808326f

Thermally induced mixing of water dominated interstellar ices

Daren J. Burke, Angela J. Wolff, John L. Edridge and Wendy A. Brown*

Received 29th April 2008, Accepted 1st July 2008
First published as an Advance Article on the web 23rd July 2008
DOI: 10.1039/b807220e

Despite considerable attention in the literature being given to the desorption behaviour of smaller volatiles, the thermal properties of complex organics, such as ethanol (C_2H_5OH), which are predicted to be formed within interstellar ices, have yet to be characterized. With this in mind, reflection absorption infrared spectroscopy (RAIRS) and temperature programmed desorption (TPD) have been used to probe the adsorption and desorption of C_2H_5OH deposited on top of water (H_2O) films of various thicknesses grown on highly oriented pyrolytic graphite (HOPG) at 98 K. Unlike many other molecules detected within interstellar ices, C_2H_5OH has a comparable sublimation temperature to H_2O and therefore gives rise to a complicated desorption profile. RAIRS and TPD show that C_2H_5OH is incorporated into the underlying ASW film during heating, due to a morphology change in both the C_2H_5OH and H_2O ices. Desorption peaks assigned to C_2H_5OH co-desorption with amorphous, crystalline (CI) and hexagonal H_2O-ice phases, in addition to C_2H_5OH multilayer desorption are observed in the TPD. When C_2H_5OH is deposited beneath ASW films, or is co-deposited as a mixture with H_2O, complete co-desorption is observed, providing further evidence of thermally induced mixing between the ices. C_2H_5OH is also shown to modify the desorption of H_2O at the ASW-CI phase transition. This behaviour has not been previously reported for more commonly studied volatiles found within astrophysical ices. These results are consistent with astronomical observations, which suggest that gas-phase C_2H_5OH is localized in hotter regions of the ISM, such as hot cores.

Introduction

Water (H_2O) is one of the most abundant molecular species observed in the interstellar medium (ISM) and is found in the form of interstellar ices frozen out on the surface of dust grains.[1] It has been well documented that interstellar dust grains play a pivotal role in the chemical and molecular evolutionary processes in the ISM.[2–4] These H_2O ice covered grains open up reaction pathways to molecules and atoms that accrete on the grains that are not available in the gas-phase. The composition of interstellar ices is dominated by H_2O, which comprises up to 60–70% of the ice,[5,6] and therefore plays a significant role in the chemistry of the ISM. Other major components within these ices include small saturated molecules such as methanol (CH_3OH) and carbon monoxide (CO). Furthermore, models predict that more complex saturated organics, such as ethanol (C_2H_5OH), which are formed *via* grain surface chemistry, are also present within these ices.[7–10] It has been estimated that the C_2H_5OH composition within these ices lies between 0.5% and 5% relative to H_2O.[9] However, infrared space observatory (ISO) data suggests the upper limit of solid C_2H_5OH to be 1.2% within these ices.[11]

The evaporation of these chemically rich icy mantles from interstellar dust grains has been shown to play a key role in the chemistry of star-forming regions in the latter stages of development, known as hot molecular cores.[12–16] Furthermore, the adsorption and desorption of astrophysical ices are also important in the sublimation and out-gassing processes of comets[17–21] and in regions where shocks lead to sudden heating of the grains.[22–24] Hence to facilitate accurate modelling of ISM processes, a detailed characterization of the adsorption and desorption of astrophysically relevant molecules from H_2O covered surfaces is essential. Despite considerable attention in the literature given to the thermal desorption of simple volatiles detected in H_2O-rich ices,[25–33] the desorption of more complex saturated molecules, such as C_2H_5OH, has yet to be explored. We have therefore used reflection absorption infrared spectroscopy (RAIRS) and temperature programmed desorption (TPD) to investigate the adsorption and desorption of C_2H_5OH from various thicknesses of amorphous solid water (ASW) grown on an underlying highly oriented pyrolytic graphite (HOPG) surface at 98 K. The exact composition of interstellar dust grains is still not accurately known and depends on the astrophysical environment. However, spectroscopic observations indicate that these grains are primarily composed of carbonaceous and silicate material.[34,35] The carbon component of these grains is known to exist in various forms including graphite, diamond and amorphous carbon.[35] Hence the HOPG substrate used in this study can be considered a suitable dust grain analogue and has previously been used to investigate the formation of small molecules on model dust grain surfaces.[36,37]

The interaction between H_2O ice films and astrophysically relevant gas-phase molecules, and the subsequent annealing of these model interstellar ices, has received considerable attention in the literature.[25–33] Such processes are of particular importance to the ISM with regards to elucidating

Department of Chemistry, University College London, 20 Gordon Street, London, UK WC1H 0AJ. E-mail: w.a.brown@ucl.ac.uk

star-formation, in addition to determining the ice composition and thermal ageing of astrophysical bodies and out-gassing kinetics.[20] Several laboratory studies have demonstrated that the thermal desorption behaviour of molecules deposited on the surface of a H_2O film, or co-deposited as a mixture, are controlled by the morphology and desorption properties of the H_2O.[25–32] H_2O ice is known to exist in a number of different phases, the physical properties of which depend on experimental factors including deposition temperature, deposition rate and the angular distribution of the impinging H_2O flux.[38–41] Deposition temperatures below $\sim$130 K lead to the formation of ASW and hence this is thought to be the dominant phase observed in the ISM.[42,43] ASW exists in two distinct phases.[39] At low temperatures ($\sim$10 K) a high density amorphous form exists. This highly porous amorphous phase undergoes an irreversible phase transition to form a low density, less porous, amorphous phase over the temperature range from 38 K–68 K.[43] When heated above the glass transition temperature (T_g = 136 K), low density ASW undergoes a structural change, transforming into a metastable liquid prior to the formation of cubic crystalline ice (CI) at 160 K.[44,45] At higher temperatures, CI converts to hexagonal ice.

There have been numerous TPD studies that have demonstrated the ability of ASW to trap astrophysically relevant molecules.[25–29,31–33] Volatile species such as CO, argon, nitrogen, oxygen, methane and carbon dioxide, all give rise to two additional high temperature features in the TPD that are independent of the adsorbate. The first of these features is ascribed to an explosive desorption process corresponding to the ASW-CI phase transition, whereby trapped molecules that are incorporated into the H_2O bulk are released from the ice *via* the opening of connected pathways to the surface.[46] The second, higher temperature, feature is assigned to co-desorption with crystalline ice. Similar effects have also been observed for adsorbates dosed beneath thick ASW films.[28,46]

In contrast, there have only been a few previous theoretical and experimental studies in the literature that have investigated binary layered C_2H_5OH/H_2O ices.[47–50] The interaction of C_2H_5OH on ice surfaces has been investigated using density functional theory calculations[47] and molecular dynamics (MD) simulations,[48] with the adsorption of C_2H_5OH on the ice surface shown to occur *via* the formation of hydrogen bonds. Thermally induced mixing of layered binary amorphous C_2H_5OH and heavy water films has been reported by Souda and co-workers.[49] Using temperature programmed time-of-flight mass spectrometry, it was shown that C_2H_5OH was not incorporated into the underlying D_2O film at 15 K. However, subsequent annealing of the binary layers showed that thermally induced mixing occurred in two phases. The onset of mixing was observed at $\sim$120 K, corresponding to a morphology change in the C_2H_5OH overlayer, leading to incomplete mixing. Complete mixing at the molecular level occurred between the layers above 140 K due to the increased mobility of the underlying D_2O film. The same authors reported almost identical behaviour for layered binary systems of CH_3OH and H_2O.[51,52] Similarly, Wolff *et al.* observed thermally induced mixing when CH_3OH was deposited on ASW films adsorbed on an HOPG substrate at 97 K.[53] TPD showed that in addition to CH_3OH monolayer and multilayer desorption, CH_3OH also exhibited a co-desorption feature with crystalline H_2O. However in this case, the mechanism was ascribed to the entrapment of CH_3OH at grain boundaries during the ASW-CI transition, rather than a complete mixing between the two films. A recent study performed by Bahr *et al.* investigated the interaction between CH_3OH and ASW adsorbed on polycrystalline Ag at 125 K.[54] Using a combination of metastable-impact-electron spectroscopy, RAIRS, TPD and MD calculations, it was shown that CH_3OH forms strong hydrogen bonds with the dangling OH bonds on the ASW surface upon adsorption. TPD data showed that when a submonolayer film of CH_3OH was deposited on top of ASW, it was not incorporated into the underlying film. However when the deposition sequence was reversed, the D_2O molecules became embedded in the underlying CH_3OH film.

In this paper we present the first detailed RAIRS and TPD study of C_2H_5OH desorption from H_2O-ice deposited on a model dust grain surface (HOPG) at 98 K. In addition, we also discuss the implications of the thermal desorption of the H_2O component of the ice, which is clearly affected by the presence of the C_2H_5OH ices. Modification of the H_2O thermal desorption profile has not previously been reported, despite numerous model interstellar ice investigations. In order to fully understand the complex thermal desorption processes of this binary system, reverse deposition experiments (*i.e.* various thicknesses of H_2O deposited on top of C_2H_5OH ices) and the adsorption of astrochemically relevant mixtures of $C_2H_5OH:H_2O$ were also investigated. Although interstellar ices are expected to form complex mixtures, there is also evidence which suggests that H_2O-rich ices may undergo segregation as the temperature of the ice increases (>80 K).[55] Hence, the investigation of layered binary ices, where C_2H_5OH is deposited on top of ASW, is relevant to the ISM and to cometary environments.[55,56] Three different thicknesses of pre-deposited H_2O films are examined and are categorized as thin, medium and thick films, corresponding to H_2O exposures of 2, 10, and 50 L. It has been previously shown that H_2O does not wet the graphite surface and forms 2D (monolayer) and 3D (monolayer + bilayer) island clusters prior to forming a complete monolayer film.[57,58] Hence, a 2 L exposure corresponds to a combination of H_2O clusters and bare patches of HOPG, a 10 L film corresponds to a saturated monolayer and a 50 L exposure leads to a thick amorphous film which undergoes a phase transition to a less porous phase (CI) prior to desorption. For clarity in the following discussion, the binary systems investigated in this study will be described as C_2H_5OH/H_2O(2 L), C_2H_5OH/H_2O(10 L) and C_2H_5OH/H_2O(50 L). This notation will also be extended to the reverse deposition systems, where H_2O is deposited on top of C_2H_5OH films, with the corresponding thickness of the C_2H_5OH film given in brackets.

Experimental

The apparatus used for the experiments reported here has been described elsewhere,[59] hence only a brief description will be given. Experiments were performed in an ultra high vacuum (UHV) apparatus with a base pressure of $\leq 2 \times 10^{-10}$ mbar. The HOPG sample was cleaned before each experiment by

annealing at 500 K in UHV for 3 minutes. Sample cleanliness was confirmed by the absence of any desorption during TPD experiments performed following no dosage. C_2H_5OH (99.7–100% AnalaR BDH) and H_2O (distilled, deionized) were used to create the binary layered ices. Both were purified by repeated freeze-pump-thaw cycles. Gas mixtures were admitted into the chamber by the use of a high precision leak valve and deposited onto the HOPG substrate held at 98 K by backfilling the chamber. All exposures are measured in Langmuir (L), where 1 L = 10^{-6} mbar s.

RAIR spectra were recorded using a Mattson Instruments RS1 Research Series Fourier transform infrared spectrometer coupled to a liquid nitrogen cooled MCT detector. All spectra were taken at a resolution of 4 cm^{-1} and are the result of the co-addition of 256 scans. For the annealed RAIRS experiments, the sample was held at a pre-determined temperature for 3 minutes before cooling back to the base temperature where a spectrum was recorded. TPD spectra were recorded with a Hiden Analytical HAL201 quadrupole mass spectrometer. The simultaneous desorption of mass 18 and mass 31, the major mass fragments of H_2O and C_2H_5OH, respectively, was recorded. All TPD spectra were recorded at a heating rate of 0.5 ± 0.01 K s^{-1}.

Results and discussion

TPD data

H_2O desorption. Fig. 1 shows a series of TPD spectra for H_2O desorption from all three binary layered systems as a function of overlayer C_2H_5OH exposure. TPD spectra arising from the C_2H_5OH/H_2O(2 L) system following low C_2H_5OH exposures see an immediate shift in desorption temperature from 142 K for 2 L of pure H_2O to 145 K for C_2H_5OH covered H_2O. The desorption temperature remains constant at 145 K for deposition of C_2H_5OH up to exposures of 20 L. However, for C_2H_5OH exposures above 20 L (corresponding to the onset of multilayer formation[60]) a progressive upward shift in desorption temperature, and a gradual sharpening of the H_2O profile, is observed. By an C_2H_5OH exposure of 300 L, the H_2O desorption profile has sharpened considerably and has a maximum desorption temperature of 154 K. As the exposure of H_2O remains constant for all of the TPD spectra shown in Fig. 1A, the area under the TPD traces should remain constant (within experimental error). However, for C_2H_5OH exposures above 100 L, there is an increase in the integrated area under the H_2O TPD traces. This is discussed below.

The desorption of a 10 L film of H_2O covered by C_2H_5OH (Fig. 1B), shows an immediate change upon C_2H_5OH adsorption. At the lowest C_2H_5OH exposures (5 L) the H_2O TPD trace sharpens compared to the pure H_2O ice and also exhibits a minor upward shift in desorption temperature from 151 K to 153 K. C_2H_5OH exposures above 50 L also see the appearance of a high temperature shoulder on the main H_2O desorption peak at 156 K, in addition to an increase in desorption temperature of the main peak to 155 K at C_2H_5OH exposures of 300 L. The high temperature feature becomes more prominent with increasing C_2H_5OH exposure. As expected, the integrated area under the H_2O TPD traces remains constant at all C_2H_5OH exposures.

In contrast to the C_2H_5OH/H_2O(2 L) and C_2H_5OH/H_2O(10 L) layered ices, H_2O desorption from the C_2H_5OH/H_2O(50 L) system, shown in Fig. 1C, remains relatively unchanged as a function of C_2H_5OH exposure, with only minor perturbations observed on the leading edge of the H_2O traces. As observed in

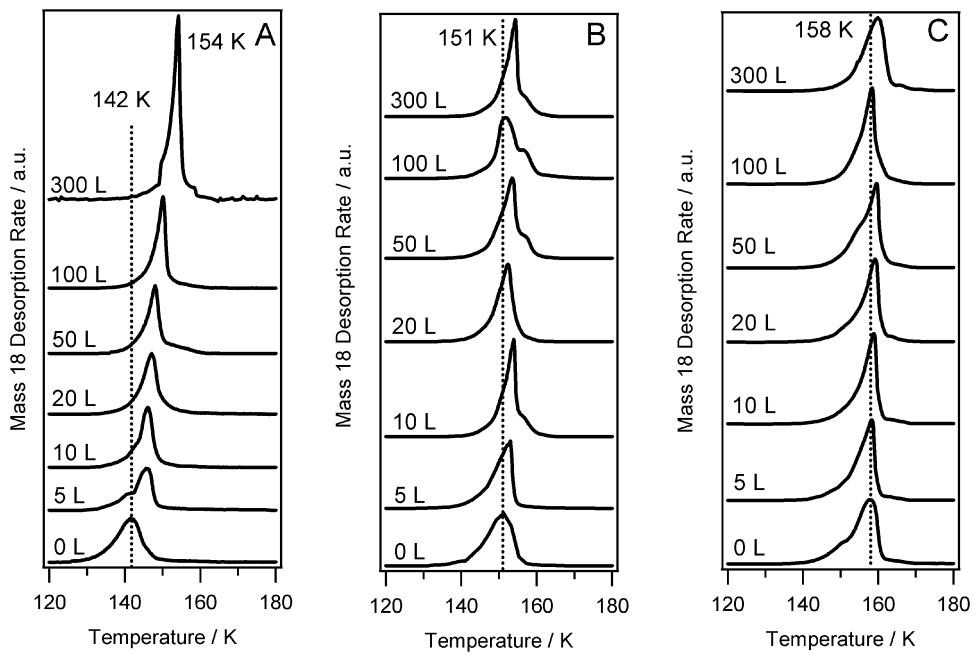

Fig. 1 TPD spectra showing the desorption of H_2O from layered binary C_2H_5OH/H_2O ices for exposures of (A) 2 L, (B) 10 L and (C) 50 L H_2O grown on HOPG at 98 K. C_2H_5OH exposures deposited onto the H_2O films are shown in the figure. TPD traces for pure H_2O ices with no C_2H_5OH overlayer are also shown.

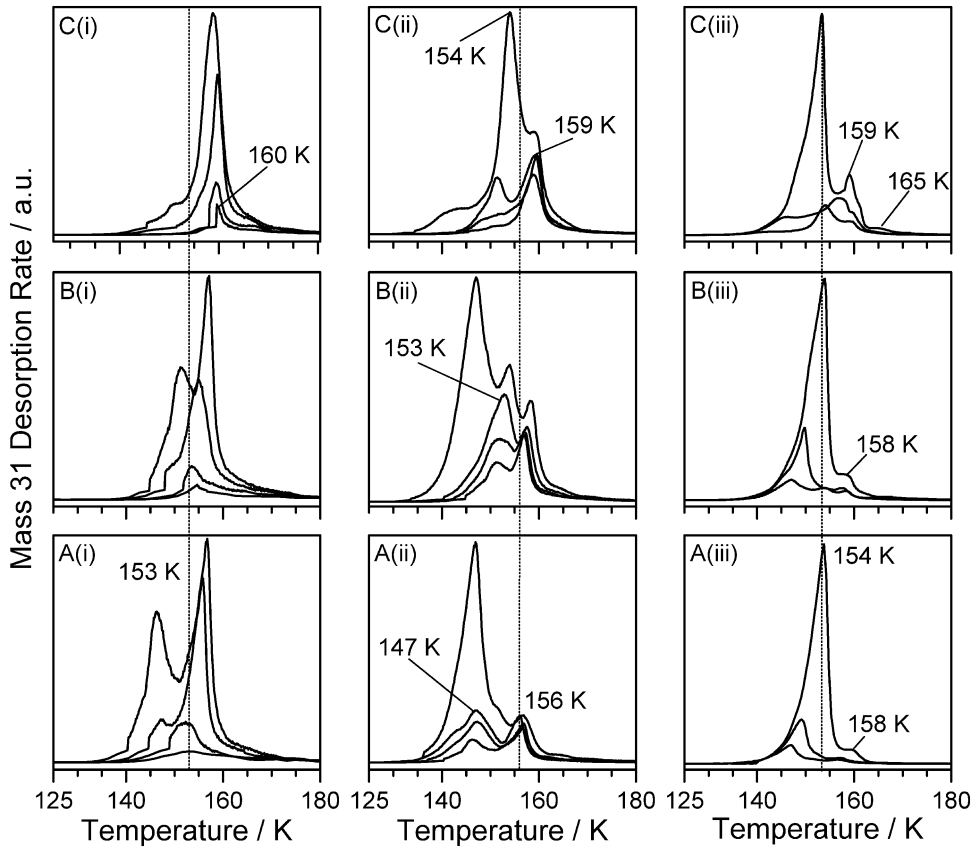

Fig. 2 TPD spectra for C_2H_5OH adsorbed on underlying H_2O films resulting from exposures of (A) 2 L, (B) 10 L and (C) 50 L H_2O adsorbed on HOPG at 98 K. Panels on the left labelled (i) show low C_2H_5OH exposures of 1, 2, 5 and 10 L. The central panels labelled (ii) show medium C_2H_5OH exposures of 10, 15, 20 and 50 L. Panels on the right labelled (iii) show high C_2H_5OH exposures of 50, 100 and 300 L.

the C_2H_5OH/H_2O(10 L) system, the integrated area under the H_2O TPD spectra remains constant across the entire C_2H_5OH exposure range. Closer comparison of the pure H_2O TPD trace with the H_2O TPD traces with an C_2H_5OH overlayer, shows that the distinctive bump on the leading edge, ascribed to the ASW-CI phase transition, is not as prominent.

Fig. 1 clearly shows that H_2O desorption is impeded by the C_2H_5OH overlayers, characterized by an upward shift in the maximum desorption temperature, in addition to the development of desorption features at higher temperatures for the C_2H_5OH/H_2O(10 L) ices. The extent of these effects is dependent on the relative thicknesses of the two films, in addition to the difference between the respective H_2O and C_2H_5OH film desorption temperatures. At low exposures (<20 L), C_2H_5OH has a tendency to form islands, hence the C_2H_5OH overlayer does not significantly inhibit H_2O desorption. However, at exposures where C_2H_5OH forms multilayers (≥ 50 L) the overlayer begins to impede H_2O desorption. Assuming that there is no mixing (or limited mixing) between the two layers, the sequential deposition of the films would prevent H_2O desorption prior to desorption of the C_2H_5OH overlayer. The desorption temperatures for C_2H_5OH when adsorbed on the H_2O ices range from 142 to 158 K for C_2H_5OH exposures of 50 L–300 L. Since the H_2O desorption temperature increases with exposure (142 K for 2 L, 151 K for 10 L and 158 K for 50 L) the thinner H_2O films exhibit a greater deviation from the pure TPD spectrum. In the case of the 2 L H_2O ice, the H_2O is held on the HOPG surface until $\sim$12 K above its normal sublimation temperature. This results in an abrupt desorption from the surface that exceeds the pumping speed of the chamber, giving rise to an artificial enhancement of the measured TPD desorption trace. Similar explosive desorption has also been reported by Wolff *et al.* for layered binary films of CH_3OH/H_2O.[53] In contrast, 50 L H_2O films, which have a comparable desorption temperature to the C_2H_5OH overlayer, remain relatively unchanged.

C_2H_5OH desorption. Fig. 2 shows a series of C_2H_5OH TPD spectra from pre-deposited H_2O films consisting of 2 L (Fig. 2A), 10 L (Fig. 2B) and 50 L (Fig. 2C) of H_2O grown on a HOPG surface exposed to increasing amounts of C_2H_5OH at 98 K. Comparing the C_2H_5OH TPD spectra for all three binary systems shown in Fig. 2, it is clear that the thickness of the underlying H_2O film has a significant effect on the C_2H_5OH desorption profile. C_2H_5OH desorption from the C_2H_5OH/H_2O(2 L) and C_2H_5OH/H_2O(10 L) ices exhibits three and four desorption species over the 300 L exposure range, respectively. TPD spectra for C_2H_5OH deposited onto a 50 L thick ASW film are characterized by a contrasting and increasingly complex desorption behaviour compared to the thinner binary films. The TPD data shown in Fig. 2 will be initially described in a general manner, before providing a detailed discussion and full assignment of the C_2H_5OH species desorbing from the model interstellar ices.

At low C_2H_5OH exposures, each binary system is characterized by a single C_2H_5OH desorption peak (153 K for the C_2H_5OH/H_2O(2 L) ice), which appears at higher temperatures with increasing thickness of the underlying H_2O ice. This peak saturates around 15 L for the C_2H_5OH/H_2O(2 L) and C_2H_5OH/H_2O(10 L) ices, desorbing at 156 and 159 K, respectively. The corresponding C_2H_5OH desorption from the 50 L H_2O ice saturates at higher C_2H_5OH exposures, desorbing at 159 K. A second, lower temperature, feature appears in the TPD spectrum at higher C_2H_5OH exposures above 5 L. This feature desorbs at 147 and 153 K for C_2H_5OH exposures of 20 L in the C_2H_5OH/H_2O(2 L) and C_2H_5OH/H_2O(10 L) binary ices, respectively. However, this peak appears at higher C_2H_5OH exposures in the C_2H_5OH/H_2O(50 L) ice, around 15 L, desorbing at 154 K for C_2H_5OH exposures of 50 L. Increasing the thickness of the underlying H_2O ice increases the dominance of this desorption feature up to C_2H_5OH exposures of 50 L. C_2H_5OH exposures of 50 L see the appearance of a third desorption peak in each TPD spectrum at $\sim$145 K. This peak is characterized by a progressive upward shift in desorption temperature and intensity with increasing C_2H_5OH exposure and dominates the TPD spectra for all three binary systems. Following an C_2H_5OH exposure of 300 L this peak is observed at $\sim$154 K. At high C_2H_5OH exposures, the C_2H_5OH/H_2O(2 L) and C_2H_5OH/H_2O(10 L) layered ices exhibit very similar TPD spectra. An additional broad feature, common for C_2H_5OH desorption from the 2 L and 10 L H_2O ices, appears on the high temperature side of the main desorption peak at around 158 K. In contrast, the C_2H_5OH/H_2O(50 L) system is characterized by a complex desorption profile in the high exposure regime.

Plotting the total integrated area under the TPD peaks shown in Fig. 2 as a function of C_2H_5OH exposure (not shown) shows that the uptake of C_2H_5OH is constant as a function of increasing exposure, suggesting that it forms physisorbed multilayers in all three binary systems, irrespective of the underlying H_2O film thickness. Furthermore, the integrated area of the TPD spectrum for every C_2H_5OH exposure for each binary system is identical within experimental error. This suggests that the changes observed in the TPD profiles at the same C_2H_5OH exposure are a result of the increased thickness of the H_2O layer and not a consequence of a change of sticking probability on bare patches of HOPG when compared to thick films of ASW.

The effects of increasing the underlying H_2O ice thickness on the desorption behaviour of C_2H_5OH are more clearly illustrated in Fig. 3. In each case, TPD spectra for C_2H_5OH adsorbed on bare HOPG have been included for comparison. C_2H_5OH desorption from each of the three binary ices gives rise to a number of different species, with some features common to all three layered ice systems. To aid clarity in the following discussion, the assignments of each species, labelled in Fig. 3, will now be given. A detailed discussion of the origin of each assignment will be give later. Peak α is assigned to the desorption of an C_2H_2OH monolayer, either from the HOPG surface or from the H_2O ice. This feature is observed for the C_2H_5OH/H_2O(2 L) and C_2H_5OH/H_2O(10 L) ices. A similar low exposure feature seen in the C_2H_5OH/H_2O(50 L) system is labelled α*. Despite this feature exhibiting

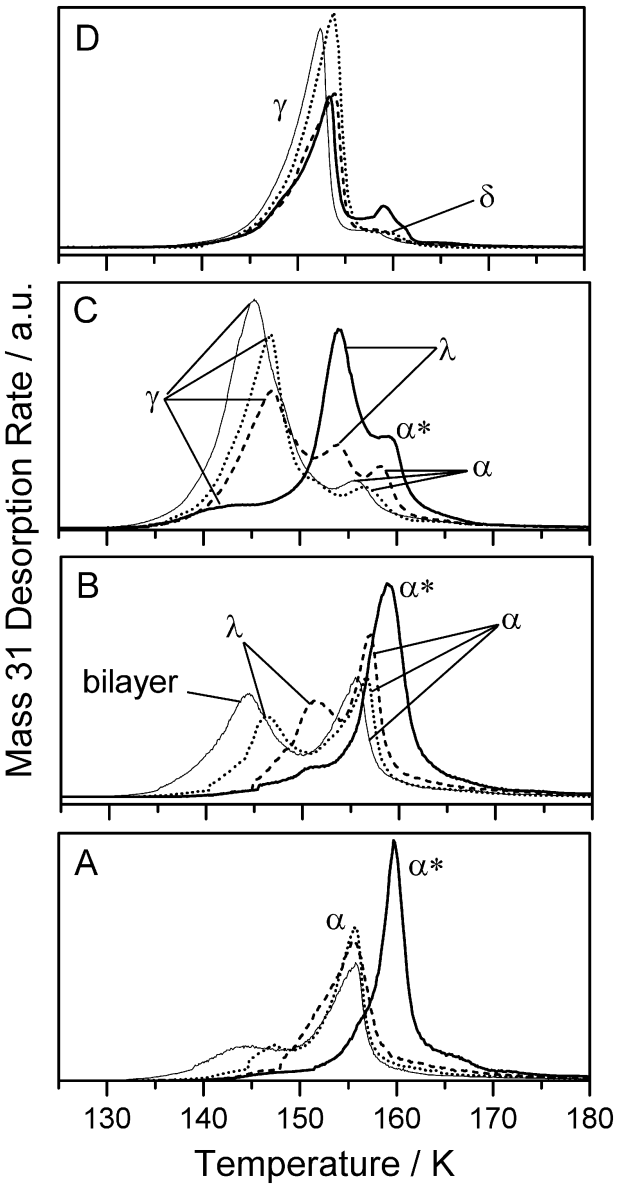

Fig. 3 Comparison of TPD spectra for C_2H_5OH adsorbed on 2 L (dotted line), 10 L (dashed line) and 50 L (thick solid line) H_2O films. C_2H_5OH desorption from a bare HOPG surface adsorbed at 98 K is also shown for comparison (thin solid line). C_2H_5OH exposures are (A) 5 L, (B) 10 L, (C) 50 L and (D) 300 L, showing the changes in the C_2H_5OH desorption features as a function of H_2O exposure.

behaviour that would initially suggest that it is of monolayer origin, closer inspection shows that this species arises from the co-desorption of C_2H_5OH and CI due to thermally induced mixing between the C_2H_5OH and H_2O layers (discussed later). Peaks γ and λ are assigned to C_2H_5OH multilayer and trapped C_2H_5OH released from ASW *via* a volcano desorption mechanism, respectively, and are common to all three layered ice systems. Peak δ is assigned to the desorption of crystalline C_2H_5OH.

The assignment of the TPD desorption features labelled δ and γ in Fig. 3C and D are made by comparing the TPD spectra arising from pure C_2H_5OH ices[60] with those for C_2H_5OH adsorbed on the H_2O ices. The broad high

temperature feature, labelled δ (Fig. 3D), which is common to the pure C_2H_5OH ices and C_2H_5OH desorption from 2 and 10 L H_2O ices, is assigned to the formation of crystalline C_2H_5OH during the heating process. This feature has been previously characterized in a RAIRS and TPD study of pure C_2H_5OH adsorption on HOPG.[60] The peak that dominates the C_2H_5OH TPD spectrum for exposures above 50 L for all three binary systems, labelled γ (Fig. 3C and D), can be confidently assigned to the desorption of multilayer C_2H_5OH. Fig. 2 shows that the onset of multilayer growth is slower with increasing H_2O film thickness and this is more explicitly shown in Fig. 3C. This effect is attributed to the change in the relative surface area of the pre-deposited H_2O films adsorbed on HOPG, which increases with H_2O exposure. As a result, a greater exposure is required to saturate the C_2H_5OH monolayer prior to formation of the multilayer as the H_2O film thickness increases. It is clear from Fig. 3C and D that the presence of H_2O on the HOPG surface modifies the desorption kinetics of multilayer C_2H_5OH compared to the pure C_2H_5OH ice. This is illustrated by an increase in the desorption temperature for peak γ for all three layered ices compared to the pure C_2H_5OH multilayer. Furthermore, the leading edges of peak γ do not overlap with those for the pure C_2H_5OH multilayer TPD spectrum, again indicating a change in the desorption kinetics. This change in the C_2H_5OH multilayer desorption kinetics probably arises from thermally induced mixing between the two layers. Overlapping the C_2H_5OH and H_2O TPD traces obtained in a single experiment for all three binary ices at C_2H_5OH exposures where peak γ is present (not shown), shows that the C_2H_5OH multilayer desorbs with the leading edge of the H_2O desorption. This implies a substantial diffusion of H_2O into the C_2H_5OH overlayer and hence a modification of the H_2O TPD profile, as evidenced in Fig. 1. This is consistent with the thermally induced mixing between C_2H_5OH and H_2O layers reported previously.[49]

Assignment of the three low temperature features for the binary ices labelled α, α* and λ in Fig. 3A, B and C is also made by comparison with the pure C_2H_5OH TPD spectra as well as by overlapping the respective C_2H_5OH and H_2O TPD spectra obtained for a single experiment. The TPD traces in Fig. 3 show that C_2H_5OH desorption from the C_2H_5OH/H_2O(2 L) layered ices exhibits very similar behaviour to that observed for the pure C_2H_5OH films. Hence peak α can be confidently assigned to the desorption of the C_2H_5OH monolayer. This assignment also holds for the C_2H_5OH/H_2O(10 L) layered ices. The broadening of the monolayer TPD profile, in addition to the increase in desorption temperature, is consistent with the increased surface area and heterogeneity of the thicker H_2O films.

The TPD data shown in Fig. 2C(i) and 3A clearly show that peak α* for the C_2H_5OH/H_2O(50 L) system exhibits different desorption behaviour to the corresponding monolayer peak observed for the thinner H_2O ices. The monolayer peak is characterized by a small increase in desorption temperature for C_2H_5OH exposures ranging from 1 L to 10 L for both the C_2H_5OH/H_2O(2 L) (Fig. 2A(i)) and C_2H_5OH/H_2O(10 L) (Fig. 2B(i)) binary ices. In contrast, Fig. 2C(i) shows that the corresponding feature in the C_2H_5OH/H_2O(50 L) ice exhibits a small decrease in temperature from 160 K to 159 K over a similar exposure range. In addition, overlapping TPD spectra for a 5 L C_2H_5OH exposure adsorbed on varying thicknesses of H_2O (Fig. 3A) shows that peak α* in the 50 L binary ice clearly desorbs at a higher temperature, whereas C_2H_5OH desorption from the thinner films closely resembles C_2H_5OH desorption from bare HOPG. This pattern is consistent for low C_2H_5OH exposures ranging from 1 to 5 L. The contrasting nature of peak α* in the C_2H_5OH/H_2O(50 L) ice is further confirmed in Fig. 4, which overlaps the corresponding C_2H_5OH and H_2O TPD spectra obtained from a 20 L C_2H_5OH exposure deposited on top of H_2O films of varying thicknesses. Fig. 4A and B clearly show that C_2H_5OH desorption assigned to peak α occurs after H_2O desorption is complete for both the C_2H_5OH/H_2O(2 L) and C_2H_5OH/H_2O(10 L) ices. However, the C_2H_5OH/H_2O(50 L) system (Fig. 4C) shows that peak α* co-desorbs with multilayer H_2O. This behaviour is consistent for all C_2H_5OH exposures in all ice configurations where peak α* is visible in the TPD spectrum. The simultaneous desorption of C_2H_5OH with H_2O in the C_2H_5OH/H_2O(50 L) binary system could either indicate co-desorption from the ASW surface or be as a result of thermally induced mixing between the two layers. Data for reverse deposition and co-deposition of H_2O and C_2H_5OH (shown later) suggest the latter assignment is the more likely and that peak α* is due to thermally induced mixing between the C_2H_5OH and H_2O layers.

Fig. 3B shows that peak λ desorbs at higher temperatures for all three binary ices when compared to the corresponding peak assigned to the C_2H_5OH bilayer observed in the pure C_2H_5OH ice.[60] Furthermore, peak λ becomes increasingly prominent in the TPD spectrum for the thicker H_2O ices, particularly at higher C_2H_5OH exposures (Fig. 3C). The contrasting behaviour of peak λ compared to the bilayer in the pure C_2H_5OH TPD spectrum (which is characterized by a peak growing into the TPD spectrum at 144 K at an C_2H_5OH exposure 5 L, before becoming obscured by multilayer growth at 25 L[60]) clearly shows that this feature is not due to the formation of an C_2H_5OH bilayer. Instead this peak must arise from an interaction between C_2H_5OH and H_2O adsorbed on the HOPG surface. Fig. 4C shows that peak λ desorbs with the leading edge of the H_2O desorption. This correlation is observed for C_2H_5OH exposures ranging from 10 L to 50 L. The bump on the leading edge of the H_2O profile corresponds to the ASW-CI phase transition for pure H_2O ices.[58,61,62] Hence, λ is assigned to a volcano desorption feature[46] whereby C_2H_5OH molecules that have become trapped in the H_2O bulk, as a result of heat induced mixing between the two layers, are released from the H_2O lattice *via* the opening of connected desorption pathways in the H_2O ice prior to crystallization. A similar volcano peak has also been observed for the desorption of CH_3OH from CH_3OH/H_2O layered ices adsorbed on HOPG at 97 K.[53]

The TPD spectra for both C_2H_5OH and H_2O shown in Fig. 4 provide evidence that C_2H_5OH thermally mixes with the H_2O overlayer prior to desorption. The existence of a trapped C_2H_5OH feature in the TPD spectra that is released, either by co-desorption with H_2O or *via* a change in morphology of the H_2O film, can only be as a result of intermixing between the

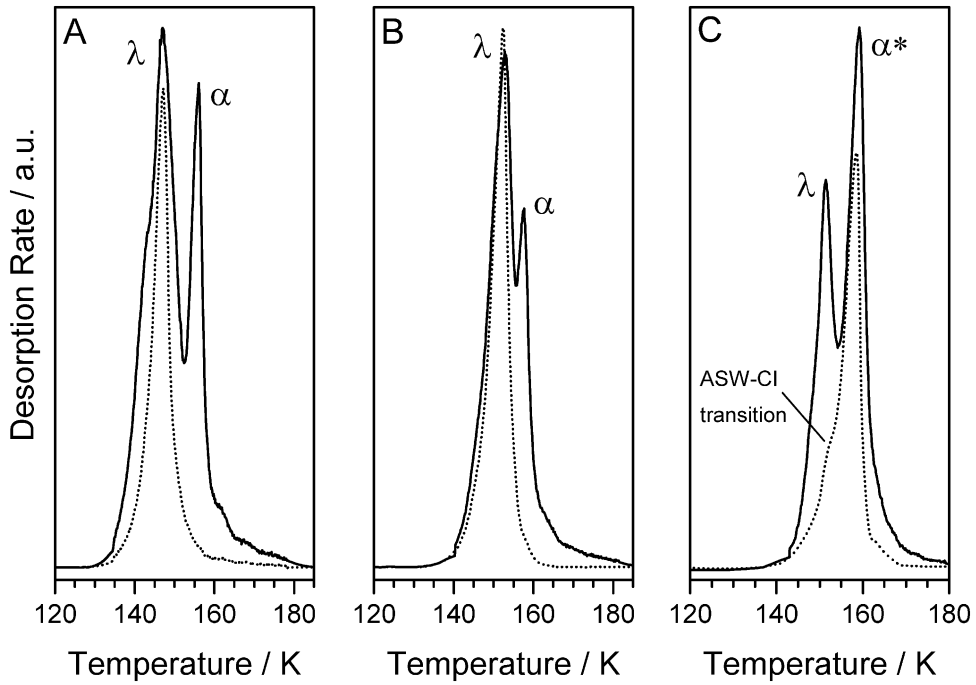

Fig. 4 TPD spectra overlaying desorption traces from a 20 L exposure of C_2H_5OH (solid lines) on top of (A) 2 L, (B) 10 L and (C) 50 L thick H_2O ices (dotted lines) adsorbed on HOPG at 98 K. The H_2O TPD spectrum in each case has been scaled for clarity.

two layers during annealing. The greater prominence of the trapped feature in the TPD spectra for the 10 L and 50 L systems (Fig. 3C) is attributed to the increased thickness of the underlying H_2O film, which has a greater capacity to trap higher volumes of C_2H_5OH during the structural rearrangement of both ice layers. However, the growth of an C_2H_5OH multilayer in the TPD, for all H_2O ice thicknesses, shows that not all of the C_2H_5OH is incorporated into the H_2O ice. This mixing also explains the appearance of the high temperature feature observed for very high exposures of C_2H_5OH ($\geq$ 100 L) in the C_2H_5OH/H_2O(50 L) system (Fig. 2C(iii)). The high temperature shoulder mirrors the desorption of the broad low intensity H_2O peak at 165 K. This feature can therefore be assigned to co-desorption of C_2H_5OH with hexagonal H_2O, which has also been observed for the co-deposited C_2H_5OH : H_2O system.[63]

In order to fully explore the dynamics of C_2H_5OH desorption and the thermally induced mixing process further, the deposition sequence was reversed, with increasing exposures of H_2O deposited on top of a saturated C_2H_5OH monolayer film (15 L) and multilayer film (50 L) grown on HOPG at 98 K (Fig. 5). Thermal processing and re-adsorption cycles, experienced in astrophysical environments as dust grains enter warm and cooler regions of the ISM, suggest that it is highly likely that segregated layers of C_2H_5OH ice could be formed under thick layers of H_2O-ice.[55] Hence reversing the deposition sequence of the binary ices is important to obtain a better understanding of the thermal processes within the ISM. It is clear from the TPD traces shown in Fig. 5 that intermixing between the two layers occurs as expected, and common trends are observed when compared to the C_2H_5OH/H_2O(50 L) system. Increasing the H_2O overlayer thickness sees a significant change in the C_2H_5OH desorption profile. For the H_2O/C_2H_5OH(15 L) films (Fig. 5A(i)), the two well defined peaks seen for the pure C_2H_5OH ice are characterized by an upward shift in temperature and develop into a single feature with a low temperature shoulder on the leading edge with increasing H_2O thickness. The desorption temperature of this feature is coincident with crystalline H_2O desorption at 160 K (Fig. 5A(ii)). Furthermore, the corresponding H_2O TPD spectra remain relatively unchanged for overlayer exposures up to 50 L (Fig. 5A(ii)). However, H_2O exposures of 100 L give rise to a sharpened CI desorption peak at 160 K with a low temperature shoulder at 155 K. The changes observed in both the C_2H_5OH and H_2O TPD traces for the H_2O/C_2H_5OH(50 L) system (Fig. 5B) are more marked, but exhibit similar trends to those shown for the H_2O/C_2H_5OH(15 L) system. The two broad C_2H_5OH desorption features observed in the pure C_2H_5OH ice resolve into two sharp well defined peaks, exhibiting increased desorption temperatures of 157 and 160 K, respectively. The H_2O TPD traces for 50 and 100 L H_2O films are also characterized by a sharpening of the CI desorption peak, in addition to the formation of a low temperature peak on the leading edge, which appears on the 100 L H_2O spectrum at 157 K.

The TPD data in Fig. 5 show that C_2H_5OH behaves differently to other astrophysically relevant molecules when deposited underneath a thick ASW film,[28,64] underlining the value of investigating more complex organic molecules that are predicted to form within interstellar ices. Previous studies have shown that some small molecules, such as CO,[64] are able to diffuse through the H_2O ice, giving rise to a low temperature feature dependent on the adsorbate sublimation temperature, in addition to desorption features corresponding to the ASW-CI transition and co-desorption with CI. For the thick H_2O overlayers, Fig. 5 shows that there is complete co-desorption

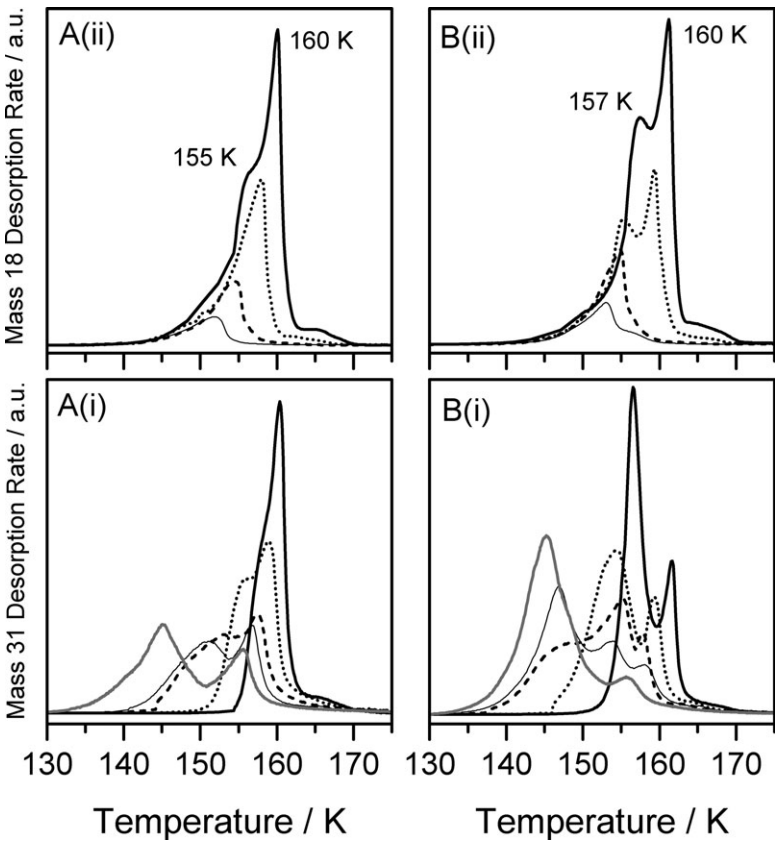

Fig. 5 TPD spectra following increasing exposures of H_2O deposited onto pre-existing C_2H_5OH films adsorbed on HOPG at 98 K. Fig. (A) shows (i) C_2H_5OH and (ii) H_2O desorption traces from a 15 L C_2H_5OH film. (B) shows the corresponding (i) C_2H_5OH and (ii) H_2O TPD arising from a 50 L C_2H_5OH film. In each case the H_2O exposures were 10 (thin solid lines), 20 (dashed lines), 50 (dotted lines) and 100 L (thick solid lines). The corresponding pure C_2H_5OH TPD traces (grey solid lines) are included for comparison.

and no evidence of desorption corresponding to the sublimation temperature of multilayer C_2H_5OH. This is more clearly seen in Fig. 6, which compares TPD spectra for 50 L C_2H_5OH exposures from both layered ice configurations and pure C_2H_5OH ices. Clearly, the diffusion process between the layers that occurs during heating leads to intermixing, whereby the H_2O/C_2H_5OH systems give similar TPD features to those observed for the C_2H_5OH/H_2O(50 L) ices. Hence, the C_2H_5OH feature desorbing at 157 K in the H_2O/C_2H_5OH(50 L) ices (Fig. 5B(i)), is coincident with the ASW-CI phase transition in the H_2O film and is therefore assigned to peak λ as seen for the C_2H_5OH/H_2O layered ices.

Fig. 6 also shows that peak α^* in the C_2H_5OH/H_2O(50 L) system overlaps with the high temperature feature observed when the deposition sequence is reversed. The correlation between the two peaks again suggests that peak α^* is not a surface co-desorption feature, but occurs as a result of thermally induced mixing between the layers. Confirmation of thermally induced mixing between the layers is also shown in the inset to Fig. 6, which compares C_2H_5OH desorption from the C_2H_5OH/H_2O(50 L) binary ice with an C_2H_5OH TPD trace obtained from the co-deposition of a mixture of $C_2H_5OH : H_2O$ (1 : 5 ratio). The resulting TPD spectra were characterized by H_2O desorption that followed identical behaviour to pure H_2O desorption, coupled with co-desorption of C_2H_5OH from the ice. The C_2H_5OH TPD spectra shown in the inset to Fig. 6 clearly show that a 10 L exposure of C_2H_5OH deposited on a 50 L H_2O film exhibits almost identical desorption behaviour to an equivalent concentration of C_2H_5OH co-deposited with H_2O. Furthermore, when overlapping the C_2H_5OH TPD spectrum from the mixtures shown in the inset to Fig. 6 with the TPD traces in the main figure, it is clear that the C_2H_5OH feature from the ice mixtures has an identical desorption temperature to peak α^* for the C_2H_5OH/H_2O(50 L) ice and the corresponding peak observed for the H_2O/C_2H_5OH(50 L) system. Hence peak α^* in the C_2H_5OH/H_2O(50 L) ice is assigned to the thermally induced mixing between the two layers. As already noted, this has previously been observed during the annealing of C_2H_5OH/D_2O binary ices.[49]

Previous studies that have focussed on the desorption of smaller molecules in interstellar ices have not reported any significant change to the H_2O desorption profile during thermal desorption experiments.[25] However, Fig. 5 clearly shows that when H_2O is deposited on top of the C_2H_5OH ice, the desorption profile is perturbed when compared to that of pure H_2O (Fig. 1C). The characteristic bump on the leading edge of the H_2O desorption profile, assigned to the ASW-CI phase transition, becomes more pronounced for the thicker H_2O films. The modification to the H_2O desorption profile suggests that the presence of C_2H_5OH within the thermally processed ice can disrupt H_2O desorption to some extent, especially if the

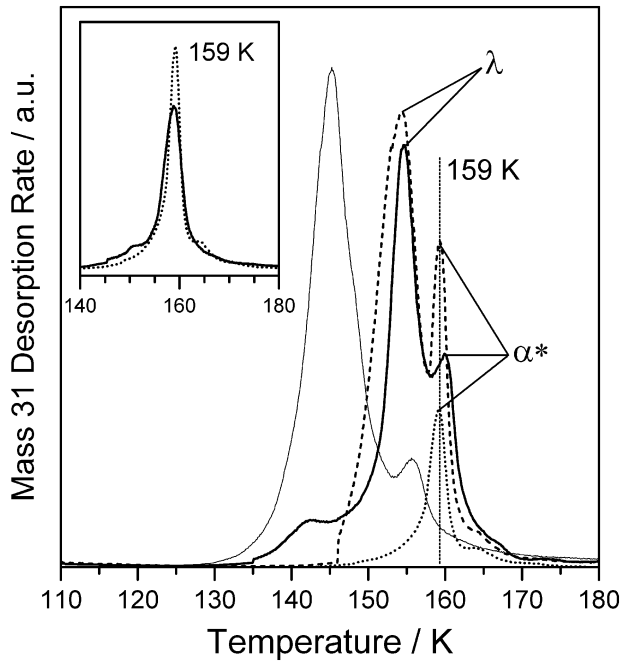

Fig. 6 TPD spectra comparing the desorption of 50 L C_2H_5OH from different ice configurations: C_2H_5OH adsorbed on top of a 50 L H_2O film (thick solid line), C_2H_5OH dosed underneath a 50 L H_2O film (dashed line) and C_2H_5OH desorption from a bare HOPG surface (thin solid line). The dotted line shows C_2H_5OH desorption from a co-deposited $C_2H_5OH:H_2O$ mixture (1 : 5 ratio) and corresponds to an equivalent exposure of 10 L of pure C_2H_5OH. The inset compares the TPD spectrum from a co-deposited $C_2H_5OH:H_2O$ mixture (dotted line) shown in the main figure to C_2H_5OH desorption from 10 L C_2H_5OH deposited on a 50 L H_2O film (solid line). In each case the substrate temperature was 98 K.

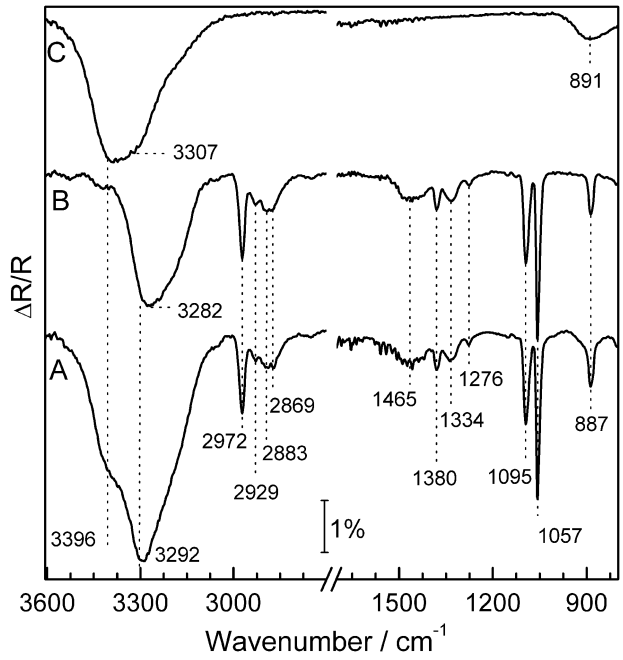

Fig. 7 Trace A shows the RAIR spectrum for a 300 L exposure of C_2H_5OH deposited on top of a 50 L H_2O film adsorbed on HOPG at 98 K. Traces B and C show RAIR spectra for pure C_2H_5OH (300 L) and pure H_2O (50 L), respectively, adsorbed on HOPG at 98 K. The region between 2700 cm^{-1} and 1700 cm^{-1}, which contains no infrared bands, has been omitted for clarity.

C_2H_5OH multilayer channel is not accessible (as in the case for the C_2H_5OH/H_2O ices). This effect has not been observed for smaller volatiles, which have been shown to diffuse through the ASW ice.

RAIRS data

C_2H_5OH adsorption on ASW. To investigate the interaction of C_2H_5OH on the ASW surface further, a series of RAIRS experiments were also performed. Fig. 7 shows a RAIR spectrum for a 300 L exposure of C_2H_5OH deposited on top of an existing 50 L H_2O ice film adsorbed on HOPG at 98 K. Fig. 7 also shows RAIR spectra for pure C_2H_5OH(300 L) and pure H_2O(50 L) ices adsorbed on bare HOPG at 98 K. The adsorption, desorption, and a full assignment of the infrared bands for both pure ices have been reported previously.[58,60] The broad band at 3396 cm^{-1}, with a low frequency shoulder at 3307 cm^{-1}, is assigned to the ν(OH) vibrational mode in the H_2O RAIR spectrum and is characteristic of the formation of ASW.[58]

It is clear that the vibrational bands and corresponding frequencies of the C_2H_5OH/H_2O(50 L) layered ice (with the exception of the broad infrared feature in the 3600–3000 cm^{-1} region of the spectrum) are almost identical to those seen for the pure C_2H_5OH ice adsorbed on HOPG.[60] Hence the infrared bands observed in the binary ice can be assigned directly to the vibrational bands seen for C_2H_5OH adsorption on HOPG. The similarity between the RAIR spectra for C_2H_5OH adsorption on HOPG and C_2H_5OH adsorbed on an ASW film implies that the ices retain a layered morphology upon adsorption at 98 K. This is further evidenced by the fact that the complex ν(OH) stretching mode in the 3600–3000 cm^{-1} region of the spectrum for the C_2H_5OH/H_2O(50 L) ice can be accurately modelled by a summation of the pure C_2H_5OH and H_2O components. The combination of the H_2O and C_2H_5OH ν(OH) frequencies leads to an upward shift of the ν(OH) band from 3282 cm^{-1} for the pure C_2H_5OH ice to 3292 cm^{-1} for the C_2H_5OH/H_2O(50 L) layered system at 98 K (Fig. 7).

Further similarities between C_2H_5OH adsorption on bare HOPG and on the ASW ice are observed during stepwise adsorption. Once the infrared bands have grown into the spectrum, increasing the C_2H_5OH exposure up to 300 L sees a corresponding increase in intensity of all bands with no associated spectral shifts. The exception to this is a noticeable broadening of the ν(OH) band on the low frequency side for exposures above 50 L, due to the increasing contribution of the C_2H_5OH ν(OH) band (observed at 3280 cm^{-1} in the pure ice). Furthermore, none of the bands saturate with increasing coverage. These observations suggest that C_2H_5OH forms physisorbed multilayers on ASW, as observed for C_2H_5OH adsorption on bare HOPG.[60] This is also in agreement with the uptake curves determined from the TPD spectra shown in Fig. 2.

There are, however, some differences with regards to the growth of the observed vibrational bands between the pure

and ASW systems during C_2H_5OH adsorption. The appearance of the band at 1382 cm^{-1}, assigned to the $\delta_s(CH_3)$ deformation, is delayed on ASW to an exposure of 50 L rather than appearing at 5 L, as on the bare HOPG surface.[60] In addition, the ν(OH) band appears immediately when C_2H_5OH is adsorbed on ASW at the lowest exposures and is characterized by a broadening of the existing ν(OH) band arising from the ASW film. For C_2H_5OH adsorbed on bare HOPG, the ν(OH) band is not observed until an exposure of 10–15 L of C_2H_5OH, which implies that the OH group is almost parallel to the surface. This suggests that at low exposures, C_2H_5OH adopts a different orientation on the ASW surface compared to adsorption on HOPG. This is expected, since ASW has dangling OH bonds at the surface, which would facilitate the formation of hydrogen bonds.[65,66] Theoretical simulations have shown that C_2H_5OH is adsorbed on the $I_h(0001)$ ice surface *via* the formation of hydrogen bonds.[47,48] Furthermore, a similar orientation change, with the hydroxyl group of CH_3OH pointing towards the dangling bonds of an ASW film, has been previously reported for submonolayer CH_3OH adsorbed on ASW films at 125 K and was attributed to the formation of hydrogen bonds.[54] However, the exact nature of the hydrogen bonding interaction between C_2H_5OH and H_2O cannot be confirmed in this study due to the inherently weaker infrared signal reflected from HOPG compared to metal surfaces. Previous studies of pure H_2O ices adsorbed on HOPG were also unable to detect the weak OH dangling bond signal.[58]

Annealing the C_2H_5OH/H_2O ices. The desorption behaviour of the binary system was investigated by performing a series of annealing experiments in order to identify the onset of thermally induced mixing observed in the TPD. Fig. 8A shows RAIR spectra for the ν(OH) band following the annealing of 300 L C_2H_5OH adsorbed on 50 L of H_2O on HOPG at 98 K. Annealing to 124 K sees the distinct high frequency shoulder at 3396 cm^{-1} smoothing out to form a single broad band at 3292 cm^{-1} with a reduced intensity. Further heating sees a continued decrease in band intensity, accompanied by a 50 cm^{-1} downshift to 3242 cm^{-1} by 150 K. By 159 K the signal has disappeared from the spectrum, indicating that both C_2H_5OH and H_2O have desorbed from the HOPG surface. The remaining infrared bands in the RAIR spectrum are characterized by a gradual decrease in intensity as the annealing temperature is increased, with no associated shifts or band splitting. All features have disappeared from the spectrum by 159 K, indicating that C_2H_5OH has desorbed from the surface.

The changes to the ν(OH) profile during annealing are in complete contrast to those observed for both pure C_2H_5OH (Fig. 8B) and pure H_2O ices. Annealing pure C_2H_5OH ices to 122 K gives rise to a sharpening of the ν(OH) vibrational mode coupled with an increase in band amplitude. Annealing to 140 K sees this band split into three different bands prior to desorption at 162 K.[60] Similar ν(OH) band splitting is also observed for the annealing of pure H_2O to 145 K.[58] In each case, these observations were ascribed to a change in morphology of the pure ices from an amorphous phase to a crystalline phase. It is evident from the data shown in Fig. 8 that annealing the binary ices does not lead to the crystallization of the C_2H_5OH ice. The RAIRS data in Fig. 8A also suggest that crystallization of the H_2O film is inhibited by the annealing process. However, the H_2O TPD data for the C_2H_5OH/H_2O(50 L) ices (Fig. 1C) are characterized by a bump on the leading edge of the main H_2O desorption peak caused by ASW crystallization.[58,61,62] Hence, it is likely that the ASW-CI phase transition in the RAIRS is obscured by the broadening of the C_2H_5OH ν(OH) vibrational band.

Similar broadening of the ν(OH) vibrational band during the annealing of binary layered CH_3OH and C_2H_5OH systems has been reported by Ayotte *et al.*[67] and was assigned to thermally induced mixing between the two layers. The observations for our C_2H_5OH/H_2O(50 L) system (Fig. 8A) can also

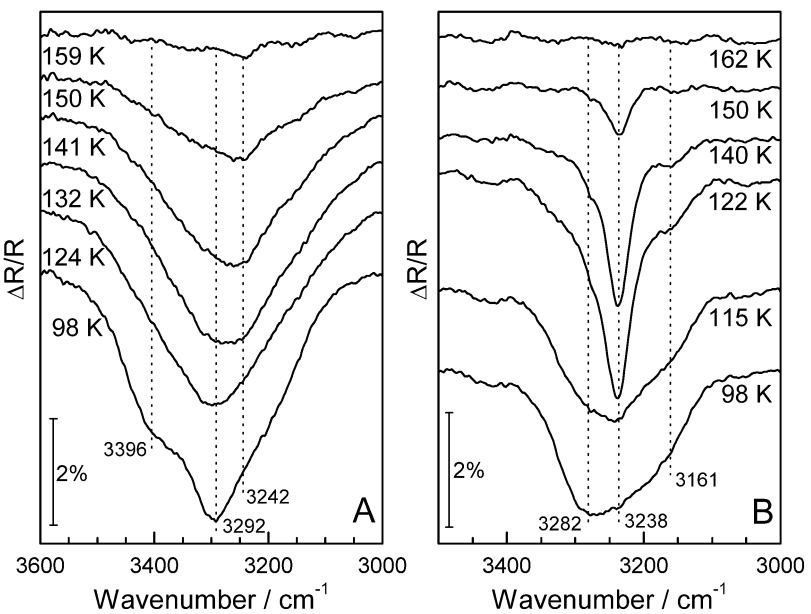

Fig. 8 RAIR spectra of the ν(O–H) stretching region from 3600 to 3000 cm^{-1}, following the sequential heating of 300 L C_2H_5OH deposited onto (A) a 50 L H_2O film adsorbed on HOPG and (B) a bare HOPG surface. The annealing temperatures are shown in the figure.

be attributed to thermally induced mixing between the C_2H_5OH overlayer and the underlying H_2O film, in agreement with the TPD data. The extent of the mixing cannot be determined by RAIRS alone. However, the TPD data presented earlier shows that mixing between the two layers is extensive enough to disrupt the crystallization of the C_2H_5OH overlayers as seen in the RAIRS.

The downshift in frequency of the ν(OH) band observed during annealing is characteristic of the formation of hydrogen bonds and suggests an interaction between the C_2H_5OH and H_2O layers that is not present during adsorption at 98 K. The interaction between the C_2H_5OH and H_2O could be a consequence of the formation of a type II clathrate hydrate, which has been previously reported in a Raman study of vapour deposition of $C_2H_5OH:H_2O$ mixtures at 88 K[68] and for CH_3OH/H_2O mixtures.[69] However this is not conclusive, since clathrates are usually formed under high pressure conditions. It is more likely that annealing leads to the formation of $C_2H_5OH:H_2O$ hydrogen bonded networks or $C_2H_5OH:H_2O$ clusters,[68] formed *via* the mutual diffusion of the ices beyond their respective glass transition temperatures. Certainly, the exact nature of the association between the C_2H_5OH and H_2O layers requires further structural analysis to accurately identify the bonding species.

Conclusions

Recent studies have shown that the thermal desorption of interstellar ices is not an instantaneous process as previously thought.[13] Hence, a better understanding of the thermal desorption of astrophysically relevant molecules adsorbed on dust grains is essential for the accurate modelling of star forming processes. Therefore a detailed RAIRS and TPD investigation of C_2H_5OH adsorption and desorption from model interstellar ices has been performed for the first time. Unlike many other molecules that are detected within interstellar ices, C_2H_5OH has a comparable sublimation temperature to H_2O, and hence gives rise to complex thermal desorption. To fully understand the complicated nature of the desorption processes, three different ice configurations have been studied, including binary layered ice systems consisting of C_2H_5OH adsorbed on top of pre-existing ASW films, layered systems where the deposition order is reversed, and intimate mixtures of $C_2H_5OH:H_2O$ ices. This study shows for the first time that H_2O desorption from a model dust grain can be affected by the presence of a complex organic molecule, such as C_2H_5OH.

Both RAIRS and TPD data show that C_2H_5OH films are incorporated into the underlying H_2O ice during the heating process. This is attributed to a morphology change in the C_2H_5OH ice, where it behaves like a viscous super-cooled fluid. As a result, C_2H_5OH co-desorbs with all three phases of the H_2O-ice: amorphous, crystalline and hexagonal ice. In the case of the thicker underlying H_2O ices, trapped C_2H_5OH molecules desorb during the ASW-CI phase transition *via* a molecular volcano mechanism. Similar C_2H_5OH co-desorption channels are also observed when reversing the deposition sequence, with H_2O adsorbed on top of C_2H_5OH ices of varying thickness. A direct comparison of the C_2H_5OH TPD from the binary ices with C_2H_5OH TPD recorded from co-deposited $C_2H_5OH:H_2O$ mixtures provides evidence to support thermally induced mixing between the layers. However, the exact nature of the interaction between the two ice films is not fully understood. The thermally induced mixing between C_2H_5OH and ASW ices shows that C_2H_5OH exhibits atypical behaviour when compared to numerous other volatiles detected within astrophysical ices. It exhibits complete co-desorption when deposited beneath ASW and when deposited as a mixture. Furthermore, C_2H_5OH is shown to modify the desorption of the H_2O ice at the ASW-CI phase transition. Such observations have not been previously reported for other astronomically relevant species, deposited either as a binary ice or co-deposited as a mixture. These findings suggest that C_2H_5OH can only be released into the gas-phase in the hotter regions of the ISM (>150 K) when the H_2O itself desorbs. This is consistent with observations of relatively high gas-phase abundances of C_2H_5OH in the vicinity of hot cores. This is in contrast to dark clouds (20 K), where gas-phase C_2H_5OH is not observed.[7–9] It is thought that the origin of these high gas-phase abundances arises from the evaporation of chemically rich icy mantles, caused by the heat generated by new born stars.

Acknowledgements

The UK EPSRC is acknowledged for PhD studentships for A.J.W. and J.L.E., in addition to an equipment and consumables grant (GR/S15273/01). The Leverhulme trust is thanked for a post-doctoral fellowship for D.J.B.. This work forms part of the research currently being undertaken in the UCL Centre for Cosmic Chemistry and Physics.

References

1. D. A. Williams, in *Dust and Chemistry in Astronomy*, eds. T. J. Millar and D. A. Williams, Institute of Physics Publishing, Bristol, 1993.
2. W. D. Watson, *Rev. Mod. Phys.*, 1976, **48**, 513–552.
3. A. G. G. M. Tielens and W. Hagen, *Astron. Astrophys.*, 1982, **114**, 245–260.
4. W. W. Duley and D. A. Williams, *Interstellar Chemistry*, Academic Press, 1984.
5. D. C. B. Whittet, in *Dust and Chemistry in Astronomy*, eds. T. J. Millar and D. A. Williams, Institute of Physics Publishing, Bristol, 1993, p. 9.
6. D. C. B. Whittet, *Dust in the Galactic Environment*, Institute of Physics Publishing, Bristol, 2003.
7. T. Millar, G. MacDonald and R. Habing, *Mon. Not. R. Astron. Soc.*, 1995, **273**, 25–29.
8. M. Ohishi, S.-I. Ishikawa, S. Yamamoto, S. Saito and T. Amano, *Astrophys. J.*, 1995, **446**, L43–L46.
9. S. B. Charnley, M. E. Kress, A. Tielens and T. J. Millar, *Astrophys. J.*, 1995, **448**, 232–239.
10. L. J. Allamandola, M. P. Bernstein, S. A. Sandford and R. L. Walker, *Space Sci. Rev.*, 1999, **90**, 219–232.
11. N. Boudin, W. A. Schutte and J. M. Greenberg, *Astron. Astrophys.*, 1998, **331**, 749–759.
12. P. Caselli, T. I. Hasegawa and E. Herbst, *Astrophys. J.*, 1993, **408**, 548–558.
13. S. Viti and D. A. Williams, *Mon. Not. R. Astron. Soc.*, 1999, **305**, 755–762.
14. H. Nomura and T. J. Millar, *Astron. Astrophys.*, 2004, **414**, 409–423.
15. P. D. Brown, S. B. Charnley and T. J. Millar, *Mon. Not. R. Astron. Soc.*, 1988, **231**, 409–417.

16. S. B. Charnley, A. G. G. M. Tielens and T. J. Millar, *Astrophys. J.*, 1992, **399**, L71–L74.
17. R. Smoluchowski, *Astrophys. J.*, 1981, **244**, L31–L34.
18. H. Patashnick, G. Rupprecht and D. W. Schuerman, *Nature*, 1974, **250**, 313–314.
19. J. Klinger, *Icarus*, 1981, **47**, 320–324.
20. J. Klinger, *Science*, 1980, **209**, 271–272.
21. A. Bar-Nun, G. Herman and D. Laufer, *Icarus*, 1985, **63**, 317–332.
22. S. Viti, P. Caselli, T. W. Hartquist and D. A. Williams, *Astron. Astrophys.*, 2001, **370**, 1017–1025.
23. J. Hatchell and S. Viti, *Astron. Astrophys.*, 2002, **381**, L33–L36.
24. M. Benedettini, J. A. Yates, S. Viti and C. Codella, *Mon. Not. R. Astron. Soc.*, 2006, **370**, 229–238.
25. M. P. Collings, M. A. Anderson, R. Chen, J. W. Dever, S. Viti, D. A. Williams and M. R. S. McCoustra, *Mon. Not. R. Astron. Soc.*, 2004, **354**, 1133–1140.
26. A. Bar-Nun, J. Dror, E. Kochavi and D. Laufer, *Phys. Rev. B*, 1987, **35**, 2427–2435.
27. A. Bar-Nun, I. Kleinfeld and E. Kochavi, *Phys. Rev. B*, 1988, **38**, 7749–7754.
28. P. Ayotte, R. S. Smith, K. P. Stevenson, Z. Dohnalek, G. A. Kimmel and B. D. Kay, *J. Geophys. Res., [Atmos.]*, 2001, **106**, 33387–33392.
29. M. P. Collings, J. W. Dever, H. J. Fraser and M. R. S. McCoustra, *Astrophys. Space Sci.*, 2003, **285**, 633–659.
30. R. L. Hudson and B. Donn, *Icarus*, 1991, **94**, 326–332.
31. G. Notesco and A. Bar-Nun, *Icarus*, 1997, **126**, 336–341.
32. O. Galvez, I. K. Ortega, B. Mate, M. A. Moreno, B. Martin-Llorente, V. J. Herrero, R. Escribano and P. J. Gutierrez, *Astron. Astrophys.*, 2007, **472**, 691–698.
33. W. A. Brown, S. Viti, A. J. Wolff and A. S. Bolina, *Faraday Discuss.*, 2006, **133**, 113–124.
34. J. S. Mathis, *Annu. Rev. Astron. Astrphys.*, 1990, **28**, 37–70.
35. B. T. Draine, *Annu. Rev. Astron. Astrphys.*, 2003, **41**, 241–289.
36. V. Pirronello, C. Liu, J. E. Roser and G. Vidali, *Astron. Astrophys.*, 1999, **344**, 681–686.
37. J. S. A. Perry and S. D. Price, *Astrophys. Space Sci.*, 2003, **285**, 769–776.
38. E. Mayer and R. Pletzer, *Nature*, 1986, **319**, 298–301.
39. K. P. Stevenson, Z. Dohnalek, R. S. Smith, G. A. Kimmel and B. D. Kay, *Science*, 1999, **283**, 1505–1507.
40. G. A. Kimmel, K. P. Stevenson, Z. Dohnalek, R. S. Smith and B. D. Kay, *J. Chem. Phys.*, 2001, **114**, 5284–5294.
41. C. Martin, C. Manca and P. Roubin, *Surf. Sci.*, 2002, **502–503**, 275–279.
42. A. Kouchi, T. Yamamoto, T. Kozasa, T. Kuroda and J. M. Greenberg, *Astron. Astrophys.*, 1994, **290**, 1009–1018.
43. P. Jenniskens and D. F. Blake, *Science*, 1994, **265**, 753–756.
44. R. S. Smith and B. D. Kay, *Nature*, 1999, **398**, 788–791.
45. R. S. Smith, Z. Dohnalek, G. A. Kimmel, K. P. Stevenson and B. D. Kay, *Chem. Phys.*, 2000, **258**, 291–305.
46. R. S. Smith, C. Huang, E. K. L. Wong and B. D. Kay, *Phys. Rev. Lett.*, 1997, **79**, 909–912.
47. C. Thierfelder and W. G. Schmidt, *Phys. Rev. B*, 2007, **76**, 195426.
48. N. Peybernes, S. Le Calve, P. Mirabel, S. Picaud and P. N. M. Hoang, *J. Phys. Chem.*, 2004, **108**, 17425–17432.
49. R. Souda, *J. Chem. Phys.*, 2005, **122**, 134711.
50. H. Kawanowa, M. Kondo, T. Shibata, Y. Gotoh and R. Souda, *Appl. Surf. Sci.*, 2004, **237**, 514–518.
51. R. Souda, H. Kawanowa, M. Kondo and Y. Gotoh, *J. Chem. Phys.*, 2003, **119**, 6194–6200.
52. R. Souda, *Phys. Rev. Lett.*, 2004, **93**, 235502.
53. A. J. Wolff, C. Carlstedt and W. A. Brown, *J. Phys. Chem. C*, 2007, **111**, 5990–5999.
54. S. Bahr, C. Toubin and V. Kempter, *J. Chem. Phys.*, 2008, **128**, 134712.
55. P. Ehrenfreund, E. Dartois, K. Demyk and L. d'Hendecourt, *Astron. Astrophys.*, 1998, **339**, L17–L20.
56. J. Crovisier, D. Bockelee-Morvan, P. Colom, N. Biver, D. Despois and D. C. Lis, *Astron. Astrophys.*, 2004, **418**, 1141–1157.
57. P. Lofgren, P. Ahlstrom, J. Lausma, B. Kasemo and D. Chakarov, *Langmuir*, 2003, **19**, 265–274.
58. A. S. Bolina, A. J. Wolff and W. A. Brown, *J. Phys. Chem. B*, 2005, **109**, 16836–16845.
59. A. S. Bolina, A. J. Wolff and W. A. Brown, *J. Chem. Phys.*, 2005, **122**, 044713.
60. D. J. Burke, A. J. Wolff, J. L. Edridge and W. A. Brown, *J. Chem. Phys.*, 2008, **128**, 104702.
61. R. J. Speedy, P. G. Debenedetti, R. S. Smith, C. Huang and B. D. Kay, *J. Chem. Phys.*, 1996, **105**, 240–244.
62. Z. Dohnalek, R. L. Ciolli, G. A. Kimmel, K. P. Stevenson, R. S. Smith and B. D. Kay, *J. Chem. Phys.*, 1999, **110**, 5489–5492.
63. D. J. Burke, A. J. Wolff, J. L. Edridge and W. A. Brown, in preparation, 2008.
64. M. P. Collings, J. W. Dever, H. J. Fraser, M. R. S. McCoustra and D. A. Williams, *Astrophys. J.*, 2003, **583**, 1058–1062.
65. J. P. Devlin and V. Buch, *J. Phys. Chem.*, 1995, **99**, 16534–16548.
66. V. Buch and J. P. Devlin, *J. Chem. Phys.*, 1991, **94**, 4091–4092.
67. P. Ayotte, R. S. Smith, G. Teeter, Z. Dohnalek, G. A. Kimmel and B. D. Kay, *Phys. Rev. Lett.*, 2002, **88**, 245505.
68. B. Chazallon, Y. Celik, C. Focsa and Y. Guinet, *Vib. Spectrosc.*, 2006, **42**, 206–214.
69. D. Blake, L. Allamandola, S. Sandford, D. Huggins and F. Freund, *Science*, 1991, **254**, 548–551.